communications physics

ARTICLE

https://doi.org/10.1038/s42005-022-01061-4 OPEN

Single-domain stripe order in a high-temperature superconductor

Gediminas Simutis[1,2✉], Julia Küspert[3], Qisi Wang[3], Jaewon Choi[4], Damian Bucher[3], Martin Boehm[5], Frédéric Bourdarot[6], Mads Bertelsen[7], Chennan N Wang[8], Tohru Kurosawa[9], Naoki Momono[9,10], Migaku Oda[9], Martin Månsson[11], Yasmine Sassa[2], Marc Janoschek[1,3], Niels B. Christensen[12], Johan Chang[3✉] & Daniel G. Mazzone[13✉]

The coupling of spin, charge and lattice degrees of freedom results in the emergence of novel states of matter across many classes of strongly correlated electron materials. A model example is unconventional superconductivity, which is widely believed to arise from the coupling of electrons via spin excitations. In cuprate high-temperature superconductors, the interplay of charge and spin degrees of freedom is also reflected in a zoo of charge and spin-density wave orders that are intertwined with superconductivity. A key question is whether the different types of density waves merely coexist or are indeed directly coupled. Here we profit from a neutron scattering technique with superior beam-focusing that allows us to probe the subtle spin-density wave order in the prototypical high-temperature superconductor $La_{1.88}Sr_{0.12}CuO_4$ under applied uniaxial pressure to demonstrate that the two density waves respond to the external tuning parameter in the same manner. Our result shows that suitable models for high-temperature superconductivity must equally account for charge and spin degrees of freedom via uniaxial charge-spin stripe fluctuations.

[1] Laboratory for Neutron and Muon Instrumentation, Paul Scherrer Institut, CH-5232 Villigen PSI, Switzerland. [2] Department of Physics, Chalmers University of Technology, SE-41296 Goteborg, Sweden. [3] Physik-Institut, Universität Zürich, Winterthurerstrasse 190, CH-8057 Zurich, Switzerland. [4] Diamond Light Source, Harwell Campus, Didcot OX11 0DE, UK. [5] Institut Laue-Langevin, 71 avenue des Martyrs, CS 20156, 38042 Cedex 9 Grenoble, France. [6] Université Grenoble Alpes, CEA, IRIG, MEM, MDN, F-38000 Grenoble cedex, France. [7] European Spallation Source ERIC, P.O. Box 176, SE-221 00 Lund, Sweden. [8] Laboratory for Muon Spin Spectroscopy, Paul Scherrer Institut, CH-5232 Villigen PSI, Switzerland. [9] Department of Physics, Hokkaido University - Sapporo, 060-0810 Sapporo, Hokkaido, Japan. [10] Department of Applied Sciences, Muroran Institute of Technology, Muroran 050-8585, Japan. [11] Department of Applied Physics, KTH Royal Institute of Technology, SE-106 91 Stockholm, Sweden. [12] Department of Physics, Technical University of Denmark, DK-2800 Kongens Lyngby, Denmark. [13] Laboratory for Neutron Scattering and Imaging, Paul Scherrer Institut, CH-5232 Villigen PSI, Switzerland. ✉email: gediminas.simutis@psi.ch; johan.chang@physik.uzh.ch; daniel.mazzone@psi.ch

A universal question in strongly correlated electron materials is how the salient degrees of freedom are microscopically coupled to stabilize novel quantum states. Unconventional superconductivity in cuprate materials is a model example, where it is thought that the macroscopic coherent quantum state arises from intertwined charge (CDW) and spin-density wave (SDW) fluctuations[1–5]. A variety of experimental results alongside theoretical Hubbard model calculations show that the ground state energies of static CDW, SDW orders and unconventional superconductivity are nearly degenerate[1,2,6–9]. However, it remains unclear how charge and spin degrees of freedom are coupled to enable high-temperature superconductivity in distinct cuprate materials.

An effective way to tune the subtle balance among the different ground states is the inclusion of holes into the copper-oxygen (Cu-O) layers, which has notably established that the density-wave orders are most stable when the number of holes per Cu site $p = 1/8$. Interestingly, this is observed concomitant with a suppression of superconductivity. In addition, in $YBa_2Cu_3O_{7-y}$, for instance, static CDW and SDW orders seem not to coexist[10,11]. This is in striking contrast with La-based cuprates where the static density-wave orders not only coexist but also show signatures of coupling[1,2,9]. Yet the two order parameters reveal very different dependencies on temperature and hole-doping. In $La_{2-x}Sr_xCuO_4$ (LSCO) with $x = p = 1/8$ the SDW order is strongest revealing an onset temperature comparable to that of superconductivity, i.e. $T_c \approx 27$ K[12], but short-range CDW order persists to temperatures above 100 K[3]. Similarly, while density-wave fluctuations exist over a broad hole-doping range in LSCO[3,13], SDW and CDW orders coexist only for $\sim 0.1 < x < \sim 0.135$ questioning whether they vanish in a common quantum critical point[3,14–18]. Summarizing, this raises the question how SDW and CDW orders are microscopically coupled, and how their fluctuations give rise to unconventional superconductivity.

To address this issue for $La_{1.88}Sr_{0.12}CuO_4$, we leverage uniaxial pressure applied along the Cu-O bond direction as a newly-established extrinsic tuning parameter. Here recent x-ray experiments[19] have demonstrated that one of the CDW domains can be suppressed through uniaxial strain. For the case of truly coupled CDW and SDW orders, we similarly expect to observe that uniaxial pressure generates a single-domain stripe SDW order (see Fig. 1). Using elastic neutron scattering with superior beam-focusing, we confirm this hypothesis and demonstrate that charge and spin orders respond to uniaxial pressure in the same manner. These results attest that adequate theories for high-temperature superconductivity must account for charge and spin degrees of freedom via uniaxial charge-spin fluctuations.

Results

The outstanding experimental challenge of our study is that sufficiently high strains may only be achieved for tiny single crystals with well-defined shapes and small surface cross-sections perpendicular to the direction of the applied pressure. Such crystals of a few mg weight are typically not suitable for neutron experiments required to unambiguously probe weak SDW order. Crucially, the scattered neutron intensity scales linearly with the crystal mass while uniaxial pressure cells generally increase background scattering, resulting in an overall insufficient signal-to-noise ratio.

To overcome this challenge, we designed a neutron study that combines three major technical advances. Firstly, we exploit new developments in neutron-ray-tracing simulations, where the Union components of the McStas suite[20] only since recently take into account background scattering processes resulting from advanced sample environments such as cryostats and pressure

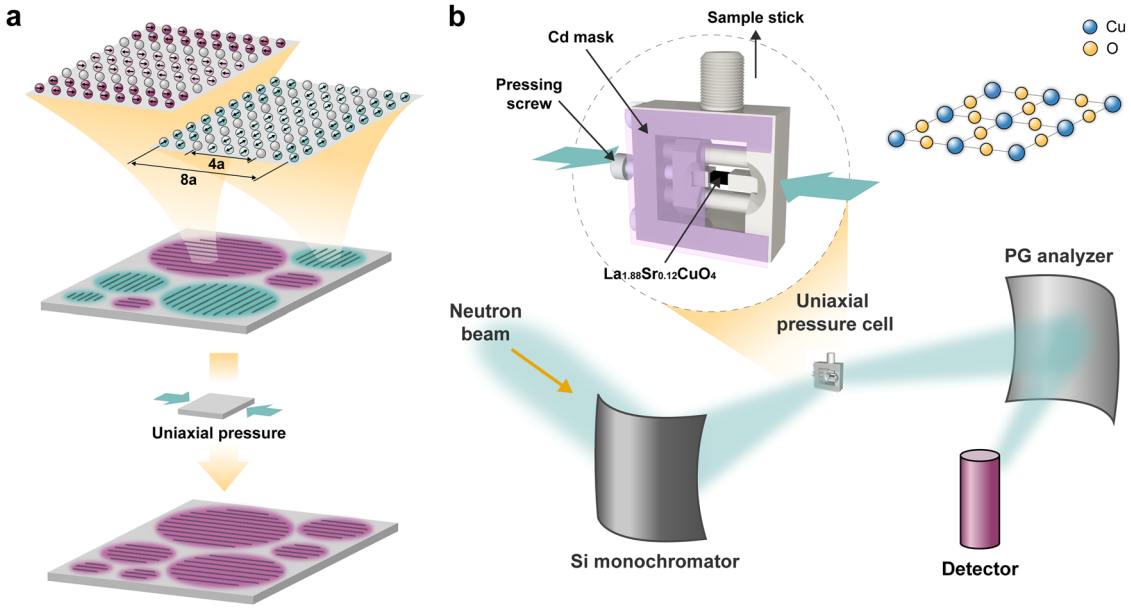

Fig. 1 Uniaxial pressure tuning of the $La_{1.88}Sr_{0.12}CuO_4$ electronic ground state. a The low-temperature ambient pressure ground state of $La_{1.88}Sr_{0.12}CuO_4$ is thought to possess equally populated charge (CDW) and spin-density wave (SDW) domains with $\delta_{CDW} = 2\delta_{SDW}$, where δ_{CDW} and δ_{SDW} are the incommensurations of the CDW and SDW wavevectors reflecting the 4*a* and 8*a* periodicity of the density waves in direct space, respectively (see also Methods section). If so, the application of uniaxial pressure should lift the ground state degeneracy, clarifying whether spin and charge degrees of freedom are intertwined in a single-domain stripe state. **b** Setup used in our neutron scattering experiment. A cuboid shaped 55 mg $La_{1.88}Sr_{0.12}CuO_4$ single crystal was mounted into a uniaxial pressure cell, and strained along the copper-oxygen (Cu-O) bond direction. The specially designed pressure cell was made of pure aluminium and masked with neutron-absorbing cadmium (Cd) to minimize background contributions. The static SDW order was studied on the cold triple-axis spectrometer ThALES at the Institut Laue-Langevin, using a double focusing silicon (Si) monochromator and pyrolytic graphite (PG) analyzer to efficiently collect neutrons diffracted from the SDW order in a ^{3}He detector.

cells. This, in turn, allowed us to optimize the signal-to-background ratio (see Supplementary Information (SI) Note 2) and demonstrate that irrespective of geometrical and instrumental details, neutrons of longer wavelengths are advantageous in terms of signal-to-noise ratio. Secondly, armed with this knowledge, we leveraged the unique focusing capabilities of the adaptive virtual source and double focusing silicon (Si(111)) monochromator at the ThALES cold neutron triple-axis spectrometer at the Institut Laue-Langevin, Grenoble, France to probe the weak SDW order in a 55 mg LSCO $x = 0.12$ single crystal[21–23]. Finally, this strongly reduced sample size (for comparison, a 1.06 g sample from the same batch was used for ambient pressure measurements. See Methods section), enabled the use of a scaled-up version of a uniaxial pressure cell, which we recently developed for x-ray studies of CDW order[19,24], without compromising uniaxial pressure application (see Fig. 1b). We note that the exquisite focusing capability of ThALES not only strongly increased the flux on the tiny sample but equally importantly reduced background scattering, allowing for a vastly improved signal-to-noise ratio (further details are given in the Methods section and in the SI Note 3).

Figure 2 shows the peaks characteristic of the SDW order in $La_{1.88}Sr_{0.12}CuO_4$ at ambient pressure and a temperature $T = 2$ K (additional scans are plotted in SI Note 5) as probed by our experiment on the 1.06 g sample. The measured count rates are shown normalized to the sample mass to facilitate a later comparison with results obtained with the pressure cell. Within the high-temperature tetragonal unit cell notation SDW order in La-based cuprates manifests as peaks at incommensurate wavevectors $\mathbf{Q}^{a}_{SDW} = (0.5 \pm \delta_{SDW}, 0.5, 0)$ and $\mathbf{Q}^{b}_{SDW} = (0.5, 0.5 \pm \delta_{SDW}, 0)$ in reciprocal lattice units (rlu). The peaks may be interpreted as the signature of either two orthogonal magnetic domains in the well-known stripe model[1,2,6,25–29] shown in Fig. 1a, or to two phase-related wavevectors describing a single-domain multi-**Q** magnetic order, which is consistent with the interpretation of earlier experimental results[28–39]. The incommensurability δ_{SDW} is doping dependent with $\delta_{SDW} \approx 0.12$ rlu around $x = 1/8$[1]. Our measurements unambiguously show that magnetic intensity is present at both wavevectors $\mathbf{Q}^{a}_{SDW}$ and $\mathbf{Q}^{b}_{SDW}$. The data were fitted with a Gaussian line shape on a sloping background, revealing an average incommensuration $\delta_{SDW} = 0.118(4)$ rlu and an in-plane correlation length $\xi_a = (a/\pi)\mathrm{FWHM}^{-1} = 67(9)$ Å, where FWHM is the full-width at half-maximum. These results are in agreement with earlier reports on $La_{1.88}Sr_{0.12}CuO_4$[12,40]. We also observe a small perpendicular incommensuration (0.007(2) rlu shown in SI Note 5), which is often referred to as Y-shift and is hypothesised to arise through pinning to orthorhombic distortions[40–42].

To probe the response of SDW order in $La_{1.88}Sr_{0.12}CuO_4$ to uniaxial pressure, we applied compressive strain $\varepsilon_a \approx 0.02\%$ (see Methods section) along the a-axis (Cu-O bond direction) of the 55 mg $La_{1.88}Sr_{0.12}CuO_4$ sample (cf. Figure 1). In Fig. 3, we display reciprocal space scans across the two wavevectors at $T = 2$ and 40 K. The high temperature data were measured above the SDW onset temperature of $T_N \approx 25$ K (see Fig. 4a, b), and used as background calibration assuming a sloping behavior. The high counting statistics enabled by our setup, allowed us to observe a magnetic signal down to approximately 2% above the background (see SI Note 6). At this level of discrimination no magnetic Bragg peak is observed at $T = 2$ K around $(-0.5 + \delta_{SDW}, 0.5, 0)$ or other symmetry equivalent reflections of $\mathbf{Q}^{a}_{SDW}$ (see SI Note 6). In strong contrast, a clear magnetic signal was found at $\mathbf{Q}^{b}_{SDW}$ (see Figs. 3 and SI Note 6). We fitted the roughly 8% strong signal at $(-0.5, 0.5 - \delta_{SDW}, 0)$ with a Gaussian lineshape over the fixed high-temperature background. The fit yields $\delta_{SDW} = 0.118(2)$ rlu and $\xi_b = 66(13)$ Å, matching the ambient pressure results. We note that a slight 0.005(1) rlu Y-shift persists under strain (see SI Note 6) and that no evidence for a pressure-induced shift in T_N is detected (see Fig. 4a, b).

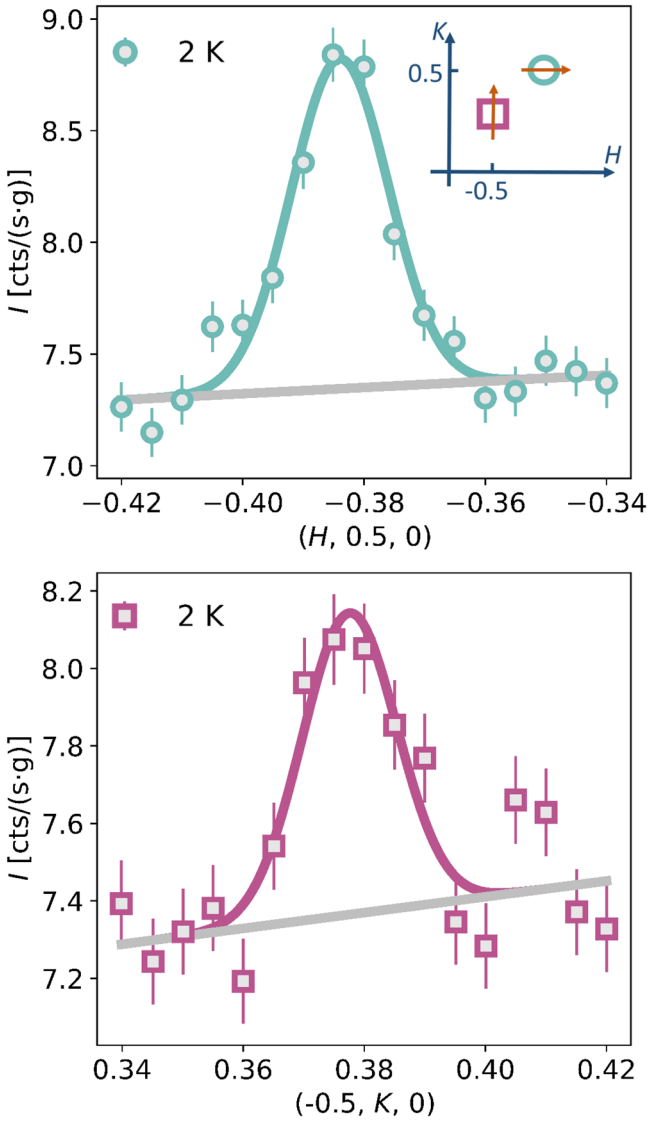

Fig. 2 Magnetic intensity under zero strain conditions. The figure displays elastic magnetic neutron scattering intensity along the two reciprocal space directions indicated in the inset. The $La_{1.88}Sr_{0.12}CuO_4$ sample was measured at ambient pressure and $T = 2$ K. Intensities (I) are given in counts (cts) per seconds (s) and mass (g) of the sample. Error bars are dictated by Poisson statistics. Scans through $\mathbf{Q}^{a}_{SDW}$ (circles) and $\mathbf{Q}^{b}_{SDW}$ (squares) reveal magnetic intensity at both wavevectors. The data were fitted with a Gaussian line shape on a sloping background.

For a quantitative comparison of the data obtained at ambient conditions and under a-axis strain, the background contributions from the scans shown in Figs. 2 and 3 were substracted. The resulting background-corrected data are displayed in Fig. 4c–f. The peaks associated with $\mathbf{Q}^{a}_{SDW}$ and $\mathbf{Q}^{b}_{SDW}$ feature integrated intensities $I_{int} = 0.030(3)$ and 0.015(3) cts·rlu/(s·g) at ambient pressure, respectively. By contrast, under uniaxial strain conditions only $\mathbf{Q}^{b}_{SDW}$ carries a finite integrated intensity of $I_{int} = 0.07(1)$ cts·rlu/(s·g). Alongside our finding that strain has no effect on the SDW ordering vector, correlation length or onset temperature, this demonstrates that uniaxial pressure along the Cu-O bond direction leads to a dramatic redistribution of magnetic peak intensity. This observation allows us to gain insight into the magnetic structure. While extrinsic tuning parameters

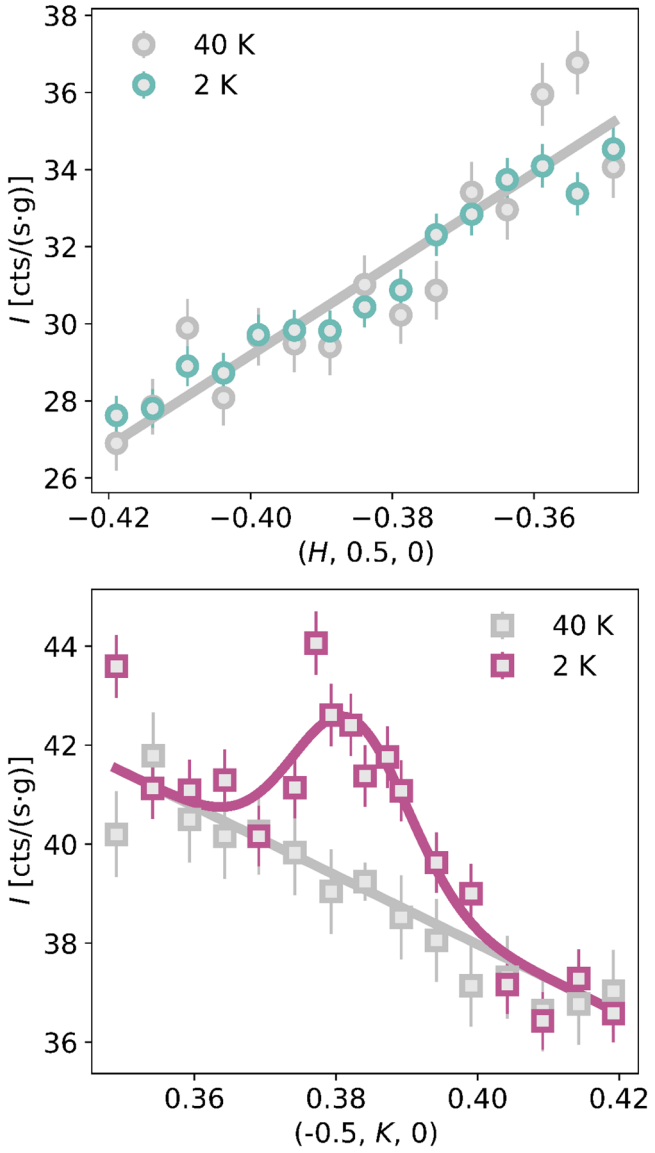

Fig. 3 Single magnetic domain state under uniaxial pressure. Reciprocal space scans of $La_{1.88}Sr_{0.12}CuO_4$ under compressive *a*-axis strain measured at $T = 2$ and 40 K. Intensities (I) are given in counts (cts) per seconds (s) and mass (g) of the sample. Error bars are dictated by Poisson statistics. Scans through $\mathbf{Q}^{a}_{SDW}$ and $\mathbf{Q}^{b}_{SDW}$ reveal a single-domain state. The high-temperature data were fitted with a sloping background. The low-temperature data for the $\mathbf{Q}^{b}_{SDW}$-domain were fitted to a Gaussian line shape over the fixed high-temperature background.

may modify the population of magnetic domains by breaking the symmetry on a macroscopic scale, they are not expected to differently affect the coexisting wavevectors in multi-**Q** structures[43,44]. Thus, our results provide direct experimental evidence for a single-**Q** magnetic structure in LSCO, and that application of pressure along one of the Cu-O directions favors the domain characterized by a propagation vector along the perpendicular Cu-O direction. We note that this effectively rules out spin-vortex checkerboard structures and any other multi-**Q** single-domain structures proposed earlier[29–33,35,37,39].

Discussion

Our observation that the application of uniaxial strain causes domain repopulation reflected in the peak intensity without altering the other characteristics of the magnetic order, demonstrates that SDW and CDW order in $La_{1.88}Sr_{0.12}CuO_4$ can be tuned by uniaxial pressure in an identical manner. Recent x-ray scattering results have shown that small uniaxial strain along the Cu-O bond direction also yields a suppression of the intensity of the CDW ordering vector along the direction of the applied pressure, and that its intensity is recovered upon strain release[19]. Together with our neutron scattering study these results strongly suggest an intertwined CDW and SDW order. Notably, this provides evidence for a charge-spin stripe arrangement (see Fig. 1a) as the fundamental density-wave state of LSCO. Theoretically, a direct coupling between static charge and spin order is supported by a microscopic mechanism in the strong coupling limit, where stripe order arises from local correlations[1,7,8,45,46]. In this picture holes are located at the antiphase SDW domain boundaries (see Fig. 1a) to minimize their kinetic energy, therefore establishing the relationship $\delta_{CDW} = 2\delta_{SDW}$ between the incommensurations of the two orders. As the direct space picture naturally connects charge and spin order, uniaxial pressure must induce a single-domain state where populated charge and spin domains are oriented along the same direction. Our observations are harder to reconcile with a weak coupling picture where the electronic order arises from Fermi surface nesting instabilities[47,48]. In this case, uniaxial pressure affects the Fermi surface topology, which would need to act similarly at $\mathbf{Q}_{SDW}$ and $\mathbf{Q}_{CDW}$ to account for a unidirectional charge and spin domain states. To explain the observation that only one ordering vector survives the pressure application, significant and peculiar anisotropic Fermi-surface distortions would be required. In contrast to our observations, one would also expect subtle shifts of the ordering wavevectors in such a scenario.

Our observation of single-**Q** charge-spin stripe order in La-based cuprates also adds to the discussion on the interplay between density-wave orders and unconventional superconductivity. Several theories attest the intertwined coupling between superconductivity and density-wave order to the emergence of a spatially-modulated superconducting order parameter that makes up for a sizable fraction of the superconducting condensate[1–3]. This putative pair-density wave (PDW) phase is thought to change sign within the spin stripes to cope with magnetic long-range order. Because both the SDW order probed here, and the CDW order explored by our previous x-ray scattering study[19] is not altered by uniaxial pressure along the Cu-O bond direction, this suggests that any PDW order will also involve uniaxial stripes. Notably, that the magnetic correlation length and SDW onset temperature, as well as the coupling between CDW order and superconductivity remain unchanged by uniaxial pressure application, suggests that in LSCO charge-spin stripe order and unconventional superconductivity are deeply intertwined. Interestingly, for $La_{2-x}Ba_xCuO_4$ (LBCO) a different behavior has been observed when uniaxial pressure is applied along an in-plane axis close to the Cu-Cu bond direction, demonstrating direct competition between superconductivity and magnetic order[49,50]. Thus, further uniaxial pressure studies on LSCO and LBCO along different crystal directions will be crucial to gain new insight into the coupling between stripe order and unconventional superconductivity.

In addition, we note that despite these differences, short-ranged charge fluctuations often exist over a wider temperature and doping range than spin order in La-based cuprates[3,14–18]. This suggests that the charge degrees of freedom are responsible for the primary fluctuations that drive the coupled charge-spin state at low temperature. Our results add further constraints to the intertwined ground state of this strongly correlated material class. They attest that adequate theories for high-temperature superconductivity must account for charge and spin degrees of freedom via uniaxial charge-spin fluctuations. Future experiments directly assessing the

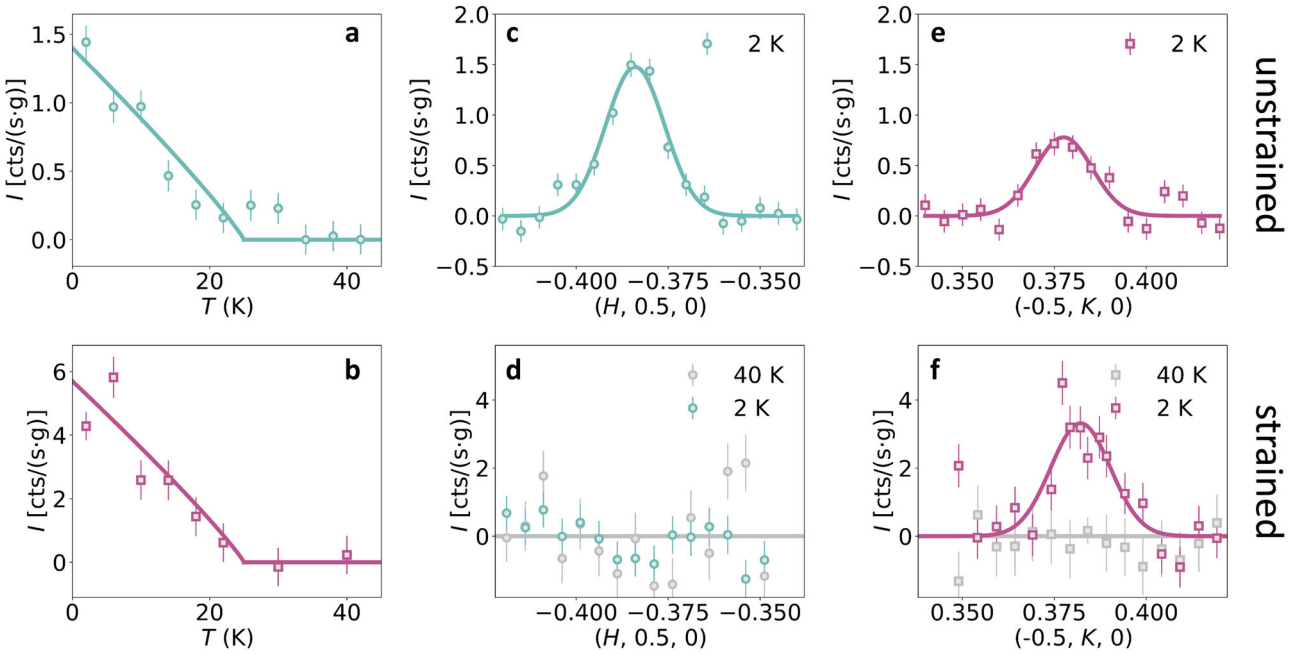

Fig. 4 Strain-induced spin-density wave domain repopulation. Background-subtracted neutron scattering results comparing the scattering from the unstrained and strained sample. The error bars are dictated by Poisson statistics and obtained via Gaussian error propagation. Panels **a** and **b** show the temperature dependence of the magnetic Bragg peak intensities at $\mathbf{Q}^{a}_{SDW}$ and $\mathbf{Q}^{b}_{SDW}$ for the unstrained and strained sample, respectively. The solid lines are guides to the eye. Panels **c** and **d** display the reciprocal space scans of $La_{1.88}Sr_{0.12}CuO_4$ around $\mathbf{Q}^{a}_{SDW}$ at ambient conditions and under compressive *a*-axis strain. In panels **e** and **f** we plot the analogous scans around $\mathbf{Q}^{b}_{SDW}$. Their comparison shows that uniaxial pressure along the $La_{1.88}Sr_{0.12}CuO_4$ copper-oxygen bond direction leads to a repopulation of the SDW domains, in which the magnetic domain perpendicular to the pressing direction is favored.

spin fluctuations under uniaxial pressure may be a fruitful way forward to gain a deeper understanding of the pairing mechanism behind high-temperature superconductivity.

Beyond the cuprates, the exact nature of the intimate coupling among various electronic degrees of freedom is crucial to the understanding of all strongly-correlated electron materials[51–53]. Our study establishes that the latest-generation neutron instrumentation allows us to explore the effects of uniaxial pressure — a particularly clean and useful tuning parameter — on spin order with weak order parameters. This advancement will be key in improving our understanding of a large range of electronic ground states. Notably, the study of coupled PDW and SDW order in heavy-fermion superconductors[54,55], coupling of ferroelectric and magnetic domains in multiferroics[53], spin, charge and lattice coupling in electronic nematic states[56–58], or the identification of topologically non-trivial multi-**Q** spin textures[59] will benefit from this capability.

Methods

Sample preparation and characterization. A high quality LSCO $x = 0.12$ crystal was grown by the travelling solvent floating zone technique. Standard magnetization measurements revealed a superconducting transition temperature $T_c = 27$ K (cf. SI Note 1). The magnetic response was checked using muon spin rotation (MuSR) at the GPS beamline of the SμS muon source, Paul Scherrer Institut, Switzerland (see SI Note 1). These measurements showed that the magnetically ordered state inside the superconducting phase is in line with the earlier studies on LSCO[12,60].

After confirming the rod's surface crystallinity by x-ray Laue diffraction, two samples of masses $m = 1.060$ and 0.055 g were oriented and cut using a tungsten wire saw. The latter sample dedicated to fit into the uniaxial pressure cell had a cuboid shape of dimensions 3.17(5)x1.35(5)x1.83(5) mm^3 along the axes of the high-temperature tetragonal unit cell. The tetragonal notation (see SI Note 1 for details) with $a = b = 3.759$ Å and $c = 13.2$ Å refined at $T = 2$ K on ThALES is employed throughout the manuscript. Here the SDW wavevector $\mathbf{Q}_{SDW}$ is shifted by $\mathbf{q}_{SDW} = (\delta_{SDW}, 0, 0)$ and $(0, \delta_{SDW}, 0)$ away from the antiferromagnetic wavevector $\mathbf{Q}_{AF} = (1/2, 1/2, 0)$. The charge order peaks at $\mathbf{Q}_{CDW}$ are offset by $\mathbf{q}_{CDW} = (2\delta_{SDW}, 0, 0)$ and $(0, 2\delta_{SDW}, 0)$ with respect to structural Bragg peaks, yielding $\delta_{CDW} = 2\delta_{SDW}$.

The bulk crystallinity of the two samples was checked using the triple-axis alignment station IN3, the neutron Laue diffractometer Orient Express and finally determined on the cold neutron spectrometer ThALES at the Institut Laue-Langevin, Grenoble, France. These data revealed that the small 55 mg sample was single crystalline within our resolution. The larger 1.06 g was composed of two crystallites shifted by 1.5 degrees with a relative intensity of 5:1 that was determined at $T = 2$ K (see SI Note 4).

A strain cell similar to those used in recent x-ray diffraction studies[19,24] was adapted to fit the cryostat dimensions of the ThALES instrument (see also Fig. 1b). We note that other neutron scattering experiments under uniaxial pressure have been performed in earlier pioneering studies[61–64]. The small ordered moment in $La_{1.88}Sr_{0.12}CuO_4$[65] required us to construct a strain cell made of high purity aluminium with an open geometry to minimize background contributions. Uniaxial pressure was applied at room temperature along the *a*-axis using an M3 aluminium screw that was rotated by 60°. Following the calibration from ref. [19]. this amounts to a compressive strain of $\varepsilon_a = \Delta a/a \approx 0.02\%$.

Neutron scattering at ThALES. The neutron scattering experiment was performed at the high-flux cold neutron spectrometer ThALES at the Institut Laue-Langevin. ThALES is uniquely suited for the purpose of our experiment since its double-focusing silicon (Si(111)) monochromator allows aggressive focusing of the incident neutron at the sample position[21–23]. This was essential to minimize parasitic scattering from the strain cell while maximizing the signal from the sample. A sketch of the experimental setup is shown in Fig. 1b. We used $k_i = k_f = 1.55$ Å^{-1} neutrons, which were cleaned from higher order contaminations via a velocity selector before the silicon monochromator and a cooled Be-filter before a double-focusing pyrolytic graphite (PG(002)) analyzer that was used to further reduce the background. The instrument was used in a *W*-configuration to minimize the extent of the instrumental resolution ellipsoid. The scattered neutrons were detected with a standard one-inch ^{3}He detector. The samples were aligned perpendicular to the (0, 0, 1) axis to access both SDW domains in the horizontal scattering plane. We improved the signal-to-noise ratio for the strain sample by optimizing the position and opening (8 mm) of the virtual slit, which is located between the velocity selector and the monochromator (see SI Note 3). Further improvements of the signal-to-noise ratio were gained through tight slit openings before (8 mm horizontal, 15 mm vertical) and after (10.5 mm horizontal, 13 mm vertical) the sample.

The temperature dependencies of the $\mathbf{Q}^{a}_{SDW}$ and $\mathbf{Q}^{b}_{SDW}$ peaks shown in Fig. 4a, b were measured on the optimized peak positions, i.e. at $\mathbf{Q} = (-0.387, 0.512, 0)$ and (-0.504, 0.382, 0), respectively. Additional reciprocal lattice scans on the 1.06 g sample were taken at intermediate temperatures to confirm the validity of the temperature dependent peak intensity measurement. Additional temperature

dependent background data on the 55 mg sample were measured at **Q** = (-0.504, 0.347, 0) and (-0.504, 0.417, 0).

Data availability

The data that support the plots within this paper are available from the corresponding authors upon reasonable request. The raw data acquired at the Institut Laue-Langevin is available via doi:10.5291/ILL-DATA.5-41-1154.

Code availability

The code used in this study is available from the authors upon reasonable request.

Received: 26 August 2022; Accepted: 27 October 2022;
Published online: 21 November 2022

References

1. Tranquada, J. M. Spins, stripes, and superconductivity in hole-doped cuprates. *AIP Conf. Proc.* **1550**, 114–187 (2013).
2. Tranquada, J. M., Dean, M. P. M. & Li, Q. Superconductivity from charge order in cuprates. *J. Phys. Soc. Jpn.* **90**, 111002 (2021).
3. Wen, J. J. et al. Observation of two types of charge density-wave orders in superconducting $La_{2-x}Sr_xCuO_4$. *Nat. Commun.* **10**, 3269 (2019).
4. Jiang, H.-C. & Devereaux, T. P. Superconductivity in the doped hubbard model and its interplay with next-nearest hopping *t′*. *Science* **365**, 1424–1428 (2019).
5. Qin, M., Schäfer, T., Andergassen, S., Corboz, P. & Gull, E. The hubbard model: A computational perspective. *Ann. Rev. Condensed Matt. Phys.* **13**, 275 (2022).
6. Kivelson, S. A. et al. How to detect fluctuating stripes in the high-temperature superconductors. *Rev. Mod. Phys.* **75**, 1201–1241 (2003).
7. Huang, E. W. et al. Numerical evidence of fluctuating stripes in the normal state of high-tc cuprate superconductors. *Science* **358**, 1161–1164 (2017).
8. Zheng, B.-X. et al. Stripe order in the underdoped region of the two-dimensional Hubbard model. *Science* **358**, 1155–1160 (2017).
9. Corboz, P., Rice, T. M. & Troyer, M. Competing states in the J-*t* model: Uniform d-wave state versus stripe state. *Phys. Rev. Lett.* **113**, 046402 (2014).
10. Blanco-Canosa, S. et al. Momentum-dependent charge correlations in $YBa_2Cu_3O_{6+\delta}$ superconductors probed by resonant x-ray scattering: Evidence for three competing phases. *Phys. Rev. Lett.* **110**, 187001 (2013).
11. Hücker, M. et al. Competing charge, spin, and superconducting orders in underdoped $YBa_2Cu_3O_y$. *Phys. Rev. B* **90**, 054514 (2014).
12. Chang, J. et al. Tuning competing orders in $La_{2-x}Sr_xCuO_4$ cuprate superconductors by the application of an external magnetic field. *Phys. Rev. B* **78**, 104525 (2008).
13. Dean, M. P. M. et al. Persistence of magnetic excitations in $La_{2-x}Sr_xCuO_4$ from the undoped insulator to the heavily overdoped non-superconducting metal. *Nat. Mater.* **12**, 1019–1023 (2013).
14. Miao, H. et al. Charge density waves in cuprate superconductors beyond the critical doping. *npj Quantum Mater.* **6**, 31 (2021).
15. Ma, Q. et al. Parallel spin stripes and their coexistence with superconducting ground states at optimal and high doping in $La_{1.6-x}Nd_{0.4}Sr_xCuO_4$. *Phys. Rev. Res.* **3**, 023151 (2021).
16. Frachet, M. et al. Hidden magnetism at the pseudogap critical point of a cuprate superconductor. *Nat. Phys.* **16**, 1064–1068 (2020).
17. Lin, J. Q. et al. Strongly correlated charge density wave in $La_{2-x}Sr_xCuO_4$ evidenced by doping-dependent phonon anomaly. *Phys. Rev. Lett.* **124**, 207005 (2020).
18. Gupta, N. K. et al. Vanishing nematic order beyond the pseudogap phase in overdoped cuprate superconductors. *Proc. Natl. Acad. Sci. USA.* **118**, e2106881118 (2021).
19. Choi, J. et al. Unveiling Unequivocal Charge Stripe Order in a Prototypical Cuprate Superconductor. *Phys. Rev. Lett.* **128**, 207002 (2022).
20. Bertelsen, M., Guidi, T. & Lefmann, K. Software for simulation and design of neutron scattering instrumentation, PhD. Thesis, University of Copenhagen, 2017.
21. Boehm, M., Hiess, A., Kulda, J., Roux, S. & Saroun, J. ThALES—three axis low energy spectroscopy at the institut laue–langevin. *Meas. Sci. Technol.* **19**, 034024 (2008).
22. Boehm, M. et al. ThALES-three axis low energy spectroscopy for highly correlated electron systems. *Neutron News* **26**, 18–21 (2015).
23. Cermak, P. et al. Optimizing monochromatic focusing on thales. *J. Phys. Soc. Jpn.* **82**, SA026 (2013).
24. Wang, Q. et al. Uniaxial pressure induced stripe order rotation in $La_{1.88}Sr_{0.12}CuO_4$. *Nat. Commun.* **13**, 1795 (2022).
25. Tranquada, J. M., Sternlieb, B. J., Axe, J. D., Nakamura, Y. & Uchida, S. Evidence for stripe correlations of spins and holes in copper oxide superconductors. *Nature* **375**, 561–563 (1995).
26. Fujita, M., Goka, H., Yamada, K., Tranquada, J. M. & Regnault, L. P. Stripe order, depinning, and fluctuations in $La_{1.875}Ba_{0.125}CuO_4$ and $La_{1.875}Ba_{0.075}Sr_{0.050}CuO_4$. *Phys. Rev. B* **70**, 104517 (2004).
27. Berg, E., Fradkin, E., Kivelson, S. A. & Tranquada, J. M. Striped superconductors: how spin, charge and superconducting orders intertwine in the cuprates. *New J. Phys.* **11**, 115004 (2009).
28. Abbamonte, P. et al. Spatially modulated 'Mottness' in $La_{2-x}Ba_xCuO_4$. *Nat. Phys.* **1**, 155–158 (2005).
29. Seibold, G., Lorenzana, J. & Grilli, M. Checkerboard and stripe inhomogeneities in cuprates. *Phys. Rev. B* **75**, 100505 (2007).
30. Christensen, N. B. et al. Nature of the magnetic order in the charge-ordered cuprate $La_{1.48}Nd_{0.4}Sr_{0.12}CuO_4$. *Phys. Rev. Lett.* **98**, 197003 (2007).
31. Fine, B. V. Magnetic vortices instead of stripes: Another interpretation of magnetic neutron scattering in lanthanum cuprates. *Phys. Rev. B* **75**, 060504 (2007).
32. Fine, B. V. Implications of spin vortex scenario for 1/8-doped lanthanum cuprates. *J. Supercond. Nov. Magn.* **24**, 1207–1211 (2011).
33. Robertson, J. A., Kivelson, S. A., Fradkin, E., Fang, A. C. & Kapitulnik, A. Distinguishing patterns of charge order: Stripes or checkerboards. *Phys. Rev. B* **74**, 134507 (2006).
34. Zachar, O., Kivelson, S. A. & Emery, V. J. Landau theory of stripe phases in cuprates and nickelates. *Phys. Rev. B* **57**, 1422–1426 (1998).
35. Aristova, A. V., Bhartiya, V. K. & Fine, B. V. Modeling superconductivity in the background of a spin-vortex checkerboard. *Phys. Rev. B* **100**, 174503 (2019).
36. Wise, W. D. et al. Charge-density-wave origin of cuprate checkerboard visualized by scanning tunnelling microscopy. *Nat. Phys.* **4**, 696–699 (2008).
37. Dolgirev, P. E. & Fine, B. V. Pseudogap and fermi surface in the presence of a spin-vortex checkerboard for 1/8-doped lanthanum cuprates. *Phys. Rev. B* **96**, 075137 (2017).
38. Wang, X., Yuan, Y., Xue, Q.-K. & Li, W. Charge ordering in high-temperature superconductors visualized by scanning tunneling microscopy. *J. Phys.: Condens. Matter* **32**, 013002 (2019).
39. Gerit Brandenburg, J. & Fine, B. V. Dimensionality of spin modulations in 1/8-doped lanthanum cuprates from the perspective of nqr and μsr experiments. *J. Supercond. Nov. Magn.* **26**, 2621–2626 (2013).
40. He, W. et al. Prevalence of tilted stripes in $La_{1.88}Sr_{0.12}CuO_4$ and the importance of *t*' in the Hamiltonian. *arXiv:2107.10264* https://arxiv.org/abs/2107.10264.
41. Kimura, H. et al. Incommensurate geometry of the elastic magnetic peaks in superconducting $La_{1.88}Sr_{0.12}CuO_4$. *Phys. Rev. B* **61**, 14366–14369 (2000).
42. Jacobsen, H. et al. Neutron scattering study of spin ordering and stripe pinning in superconducting $La_{1.93}Sr_{0.07}CuO_4$. *Phys. Rev. B* **92**, 174525 (2015).
43. Rodrguez-Carvajal, J. & Villain, J. Magnetic structures. *Comptes Rendus Phys.* **20**, 770–8025 (2019).
44. Wills, A. Magnetic structures and their determination using group theory. *J. Phys. IV Fr.* **11**, Pr9–133–Pr9–158 (2001).
45. Miao, H. et al. Formation of incommensurate charge density waves in cuprates. *Phys. Rev. X* **9**, 031042 (2019).
46. Miao, H. et al. Incommensurate phonon anomaly and the nature of charge density waves in cuprates. *Physi. Rev. X* **8**, 011008 (2018).
47. Grüner, G. The dynamics of charge-density waves. *Rev. Mod. Phys.* **60**, 1129–1181 (1988).
48. Grüner, G. The dynamics of spin-density waves. *Rev. Mod. Phys.* **66**, 1–24 (1994).
49. Guguchia, Z. et al. Using uniaxial stress to probe the relationship between competing superconducting states in a cuprate with spin-stripe order. *Phys. Rev. Lett.* **125**, 097005 (2020).
50. Kamminga, M. E. et al. Evolution of magnetic stripes under uniaxial stress in $La_{1.885}Ba_{0.115}CuO_4$ studied by neutron scattering. *arXiv:2203.00558* (2022).
51. Paschen, S. & Si, Q. Quantum phases driven by strong correlations. *Nat. Rev. Phys.* **3**, 9–26 (2021).
52. Elbio, D. Complexity in strongly correlated electronic systems. *Science* **309**, 257–262 (2005).
53. Fiebig, M., Lottermoser, T., Meier, D. & Trassin, M. The evolution of multiferroics. *Nat. Rev. Mater.* **1**, 16046 (2016).
54. Gerber, S. et al. Switching of magnetic domains reveals spatially inhomogeneous superconductivity. *Nat. Phys.* **10**, 126–129 (2014).
55. Kim, D. Y. et al. Intertwined orders in heavy-fermion superconductor $CeCoIn_5$. *Phys. Rev. X* **6**, 041059 (2016).
56. Ronning, F. et al. Electronic in-plane symmetry breaking at field-tuned quantum criticality in $CeRhIn_5$. *Nature* **548**, 313–317 (2017).

57. Fobes, D. M. et al. Tunable emergent heterostructures in a prototypical correlated metal. *Nat. Phys.* **14**, 456–460 (2018).
58. Fernandes, R. M., Chubukov, A. V. & Schmalian, J. What drives nematic order in iron-based superconductors? *Nat. Phys.* **10**, 97–104 (2014).
59. Fert, A., Reyren, N. & Cros, V. Magnetic skyrmions: advances in physics and potential applications. *Nat. Rev. Mater.* **2**, 17031 (2017).
60. Savici, A. T. et al. Muon spin relaxation studies of incommensurate magnetism and superconductivity in stage-4 $La_2CuO_{4.11}$ and $La_{1.88}Sr_{0.12}CuO_4$. *Phys. Rev. B* **66**, 014524 (2002).
61. Dhital, C. et al. Effect of uniaxial strain on the structural and magnetic phase transitions in $BaFe_2As_2$. *Phys. Rev. Lett.* **108**, 087001 (2012).
62. Liu, P. et al. In-plane uniaxial pressure-induced out-of-plane antiferromagnetic moment and critical fluctuations in $BaFe_2As_2$. *Nat. Commun.* **11**, 5728 (2020).
63. Sun, D. et al. Magnetic frustration and spontaneous rotational symmetry breaking in $PdCrO_2$. *Phys. Rev. B* **100**, 094414 (2019).
64. Sun, D. et al. Heisenberg spins on an anisotropic triangular lattice: $PdCrO_2$ under uniaxial stress. *New. J. Phys.* **12**, 123050 (2019).
65. Wakimoto, S., Birgeneau, R. J., Lee, Y. S. & Shirane, G. Hole concentration dependence of the magnetic moment in superconducting and insulating $La_{2-x}Sr_xCuO_4$. *Phys. Rev. B* **63**, 172501 (2001).

Acknowledgements

We acknowledge enlightening discussions with K. Lefmann and his group, and K. Beauvois and A. Piovano for assistance at the Institut Laue-Langevin, Grenoble. We thank the Institut Laue-Langevin for the allocated beamtime on IN22 (CRG-2807) and ThALES (5-41-1154), and the Paul Scherrer Institut for the beamtime at GPS. This work was additionally supported by the Swiss State Secretariat for Education, Research and Innovation (SERI) through a CRG-grant. The project has received funding from the European Union's Horizon 2020 research and innovation program under the Marie Sklodowska-Curie grant agreement No 884104 (PSI-FELLOW-III-3i). J. K., Q. W., and J. C. acknowledge support from the Swiss National Science Foundation (200021188564). J.K. is further supported by the PhD fellowship from the German Academic Scholarship Foundation. N.B.C. thanks the Danish Agency for Science, Technology, and Innovation for funding the instrument center DanScatt and acknowledges support from the Q-MAT ESS Lighthouse initiative. M.M. is funded by the Swedish Research Council (VR) through a neutron project grant (Dnr. 2021-06157), the Swedish Foundation for Strategic Research (SSF) within the Swedish national graduate school in neutron scattering (SwedNess), the Carl Tryggers Foundation for Scientific Research (CTS-18:272), as well as the KTH Materials Platform.

Author contributions

D.G.M. and J.C. initiated the project and planed it together with G.S., M.J., and N.B.C.. The sample was grown by M.O., N.M. and T.K., and prepared by J.K. and Q.W.. The uniaxial pressure cell was designed by D.B. and M.B. conducted the McStas simulations. G.S., M.B., F.B., C.N.W., M.M, Y.S., M.J. N.C.B, J.C. and D.G.M performed the experiments. The data were analyzed by G.S., J.Choi and D.G.M.. G.S., D.G.M., M.J. N.B.C. and J.C. wrote the paper with inputs from all co-authors.

Competing interests

The authors declare no competing interests.

Additional information

Supplementary information The online version contains supplementary material available at https://doi.org/10.1038/s42005-022-01061-4.

Correspondence and requests for materials should be addressed to Gediminas Simutis, Johan Chang or Daniel G. Mazzone.

Peer review information *Communications Physics* thanks the anonymous reviewers for their contribution to the peer review of this work. Peer reviewer reports are available.

Reprints and permission information is available at http://www.nature.com/reprints

Publisher's note Springer Nature remains neutral with regard to jurisdictional claims in published maps and institutional affiliations.